

Deep Learning for Imaging Flow Cytometry: Cell Cycle Analysis of Jurkat Cells

Philipp Eulenberg^{1,2,❸}, Niklas Köhler^{1,2,❸}, Thomas Blasi¹, Andrew Filby³, Anne E. Carpenter⁴, Paul Rees^{4,5}, Fabian J. Theis^{1,6,*}, F. Alexander Wolf^{1,**}

1 Helmholtz Zentrum München – German Research Center for Environmental Health, Institute of Computational Biology, Neuherberg, Munich, Germany.

2 Department of Physics, Arnold Sommerfeld Center for Theoretical Physics, LMU München, Munich, Germany.

3 Flow Cytometry Core Facility, Faculty of Medical Sciences, Newcastle University, Newcastle upon Tyne, UK.

4 Imaging Platform at the Broad Institute of Harvard and Massachusetts Institute of Technology, Cambridge, Massachusetts, USA.

5 College of Engineering, Swansea University, Singleton Park, Swansea, UK.

6 Department of Mathematics, TU München, Munich, Germany.

❸ These authors contributed equally to this work.

* fabian.theis@helmholtz-muenchen.de ** alex.wolf@helmholtz-muenchen.de

Abstract

Imaging flow cytometry combines the fluorescence sensitivity and high-throughput capabilities of flow cytometry with single-cell imaging, and hence provides high-volume data well-matched to the strengths of deep learning. We present DeepFlow, a data analysis workflow for imaging flow cytometry that combines deep convolutional neural networks with non-linear dimension reduction. DeepFlow uses learned features of the neural network to visualize, organize and biologically interpret single-cell data. Dissecting the cell cycle as a source of cell-to-cell variability is crucial for quantitative single-cell biology. We demonstrate DeepFlow for a large dataset of cell-cycling Jurkat cells. First, we reconstruct the cells' continuous progression through cell cycle from raw image data. This shows that DeepFlow can learn a continuous distance measure between categorical phenotypes. Second, we are able to detect and separate a subpopulation of dead cells, although the data set had been cleaned using established approaches. DeepFlow detects this morphologically abnormal subpopulation in an unsupervised manner. Third, in label-free classification of cell cycle phases, we reach a 6-fold reduction in error rate as compared to a recent approach based on boosting on a series of image features. In contrast to previous methods, DeepFlow's predictions are fast enough to consider integration with the imaging flow cytometry measurement process.

Author Summary

We present DeepFlow, a deep learning based data analysis workflow optimized for the requirements of imaging flow cytometry. We use it to analyze a large data set of a certain type of human T cells (Jurkat cells), which undergo cell cycle. DeepFlow enables reconstructing the continuous cell cycle progression of these cells, and separates dead from living cells. We show how learned features of the neural network can be visualized and biologically interpreted. When used to classify the cell cycle stage, DeepFlow performs significantly better than previous approaches.

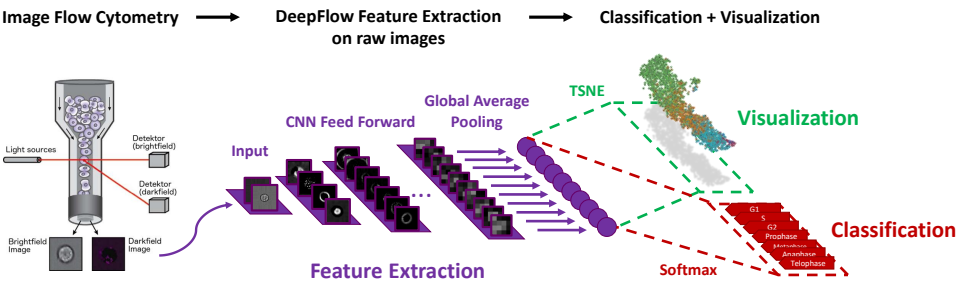


Fig 1. Overview of DeepFlow — deep learning data analysis for imaging flow cytometry. Images from all channels of the Imaging Flow Cytometer are uniformly resized, and input directly into the neural network, which is trained on the classification task. The learned features serve for both the classification objective and the visualization task.

Introduction

A major current challenge and opportunity in biology is interpreting the increasing amount of information-rich and high-throughput single-cell data. Here, we consider imaging data from fluorescence microscopy [1], in particular from imaging flow cytometry [2]. Imaging flow cytometry (IFC) combines the fluorescence sensitivity and high-throughput capabilities of flow cytometry with single-cell imaging. Relevant fluorescent labels are chosen to assess certain phenotypes of interest. The large number of single cells analyzed per sample — often hundreds of thousands — makes imaging flow cytometry unusually well-suited to deep learning, which demands very large training sets.

Further, IFC generates high-dimensional information for each cell, including spatially-mapped intensity information for thousands of pixels for each of several channels: brightfield and darkfield (which require no staining procedure) and, optionally, several fluorescence channels. This means a dramatic increase in information content as compared to the measurement of a single spatially integrated fluorescence intensity value for each channel, as in conventional flow cytometry [3]. Finally, IFC provides one image for each single cell, and hence does not require whole-image segmentation.

It is often not known in advance which morphological features are useful to distinguish specific, often rare, phenotypes in IFC. Classical computer vision algorithms are unlikely to extract sufficient metrics to capture all relevant morphological features. Deep learning, by contrast, potentially captures many more subtleties of image data. Here, we present the deep learning based data analysis workflow DeepFlow — deep learning for imaging flow cytometry. It consists of a deep convolutional neural network combined with a standard softmax classifier and a visualization tool based on non-linear dimension reduction (Fig. 1).

DeepFlow enables improved data analysis capabilities for IFC as compared to prior traditional machine learning methods [4–7]. This is mainly due to three general advantages of deep learning over traditional machine learning: there is no need for cumbersome preprocessing and manual feature definition, classification accuracy is improved and learned features can be visualized to uncover their biological meaning. Other recent work on deep learning in high-throughput microscopy either relied on engineered features [8], focused on whole-image segmentation without addressing visualization of network features [9]. Reference [10] is most closely related to the present work, but neither presents an optimized solution to Imaging Flow Cytometry data, nor

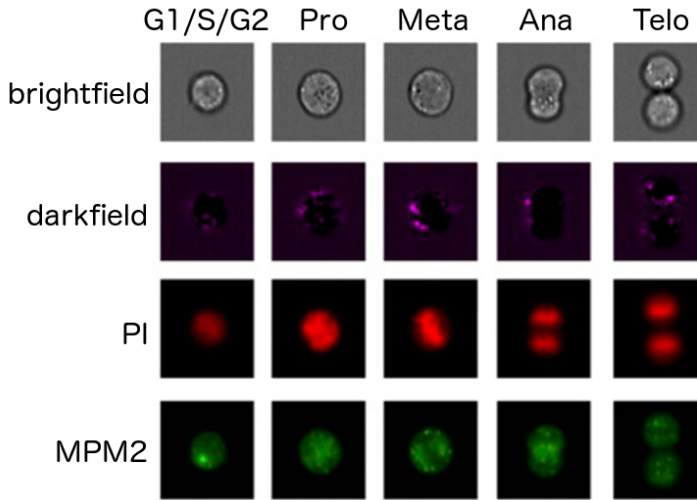


Fig 2. Representative images for the cell cycle stages as measured in brightfield, darkfield and fluorescence channels. Seven cell cycle stages define seven classes. We only show one representative image for the interphase classes G1, S, and G2, which can hardly be distinguished by eye.

addresses the particular challenges of a continuous biological process, like cell cycle. 78

Materials and Methods

We used a data set of 32,266 asynchronously growing immortalized human T lymphocytes (Jurkat cells), which had previously been analyzed using traditional machine learning [5, 11]. Images of these cells can be classified into seven different stages of cell cycle (Figure 2), including phases of interphase (G1, S and G2) and phases of mitosis (Prophase, Anaphase, Metaphase and Telophase). In this data set, ground truth is based on the inclusion of two fluorescent stains: propidium iodine (PI) to quantify each cell's DNA content and the mitotic protein monoclonal #2 (MPM2) antibody to identify cells in mitotic phases. These stains allow each cell to be labeled through a combination of algorithmic segmentation, morphology analysis of the fluorescence channels, and user inspection [5]. Note that 97.78% of samples in the dataset belong to one of the interphase classes G1, S and G2. The strong class imbalance in the dataset is related to the fact that interphase lasts — when considering the actual length of the biological process — a much longer period of time than mitosis.

Recent advances in deep learning have shown that deep neural networks are able to learn powerful feature representations [12–15]. For DeepFlow, we adapt the widely used “Inception” architecture [14], and optimize it for treating the relatively small input dimensions that occur in IFC data. The architecture consists in 13 three-layer “dual-path” modules (Suppl. Fig. 7), which process and aggregate visual information at an increasing scale. These 39 layers are followed by a standard convolution layer, a fully connected layer and the softmax classifier. Training this 42-layer deep network does not present any computational difficulty, as the first three layers consist in “reduction dual-path” modules (Suppl. Fig. 7), which strongly reduce the original input dimensions prior to convolutions in the following “normal dual-path modules”. The number of kernels used in each layer increases towards the end, until 336 feature maps with size 8 × 8 are obtained. A final average pooling operation melts the local resolution of these

maps and generates the last 336-dimensional layer, which serves as an input for both classification and visualization. The neural network operates directly on the uniformly resized images from an arbitrary number of channels of the Imaging Flow Cytometer. It is trained with cell images that have been labeled as described above, using stochastic gradient descent with standard parameters (see Suppl. Notes). Here, we focus on the case in which only the brightfield and darkfield channels are used as input for the network, during training, visualization and prediction. This case is interesting as sometimes fluorescent labeling might affect the biological process under study and should then be avoided. Also, this case provides much less information as when using all channels, and hence provides a difficult benchmark test for DeepFlow. We note, however, that technical imperfections in the IFC data capture might always lead to a minor amount of fluorescence signal, activated by a fluorescence channel, in the darkfield and brightfield channels, a phenomenon known as “bleed through” (see Suppl. Notes).

Results

To show how learned features of the neural network can be used to visualize, organize and biologically interpret single-cell data, we study the activations in the last layer of the neural network [10, 16]. We refer to this as studying the *activation space representation* of the data. The approach is motivated by the fact that the neural network strives to organize data in the last layer in a linearly separable way, given that it is directly followed by a softmax classifier. Euclidian distances in this space can be interpreted as similarities between cells in terms of the features extracted by the network. Cells with similar feature representations — and hence similar class assignments — are close to each other in Euclidian distance and cells with different class assignments are far away from each other.

Still, the activation space of DeepFlow’s last layer has 336 dimensions; it is much too high-dimensional to be accessible for human interpretation. As the fine-grained geometric structure of data in this space is highly complex, non-linear dimension reduction methods are best suited to visualize the data in a lower dimensional space. We thus use t-distributed stochastic neighbor embedding (tSNE) [17] to visualize the activation space representation [16] of a validation data set.

DeepFlow reconstructs continuous cell cycle progression.

In this visualization, we observe that the Jurkat cell data is organized in a long stretched cylinder along which cell cycle phases are ordered in the chronologically correct order (Fig. 3a). This is remarkable as the network has been provided with neither structure within the class labels nor the relation among classes but simply with categorical class labels. The learned features evidently allow reconstructing the continuous temporal progression from the raw IFC data, and by that allow defining a continuous distance between the phenotypes of different cell cycle phases.

We separately visualized just those cells annotated as being in the interphase classes (G1, S, G2) (Figure 3b). We overlaid on this structure a color map displaying the DNA content of cells as obtained after segmentation of images from one of the fluorescent channels (PI). The DNA content reflects the continuous progression of cells in the cell cycle on a more fine-grained level. Its correspondence with the longitudinal direction of the cylinder found by tSNE demonstrates that the temporal order learned by the neural network is accurate even beyond the categorical class labels.

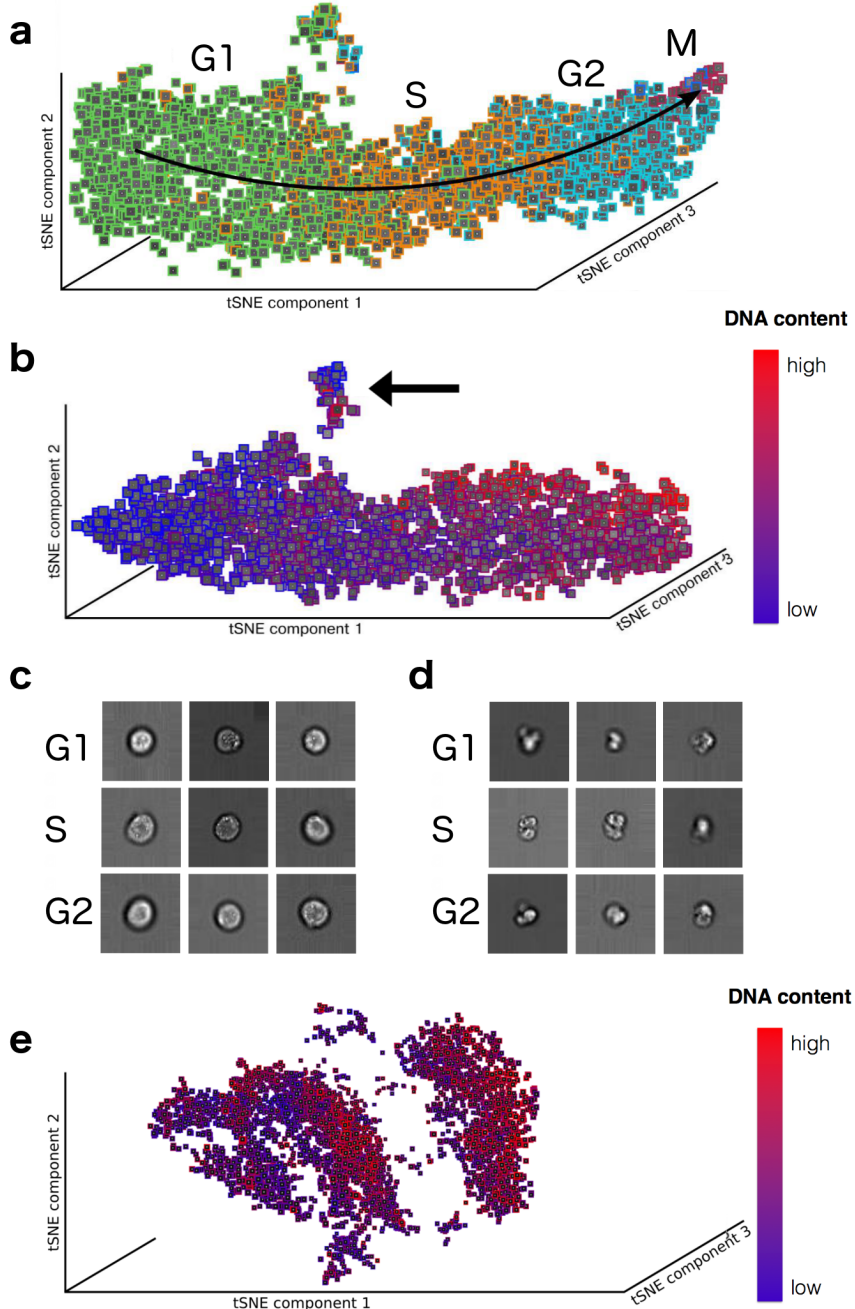


Fig 3. Visualization. **a**, tSNE visualization of test set data in activation space representation. All interphase classes (G1, S, G2) and the two mitotic phases with the highest number of representatives are shown (Prophase: red, Metaphase: blue). Telophase and Anaphase are not visible due to their low number representatives. **b**, tSNE visualization of data from the interphase classes (G1, S, G2) in activation space. The color map now shows the DNA content of cells. A cluster of damaged cells is indicated with an arrow. **c**, Randomly picked representatives from the bulk of undamaged cells. **d**, Randomly picked representatives from the cluster of damaged cells. **e**, tSNE visualization of data from the interphase classes (G1, S, G2) in the space of features used in Ref. [5]

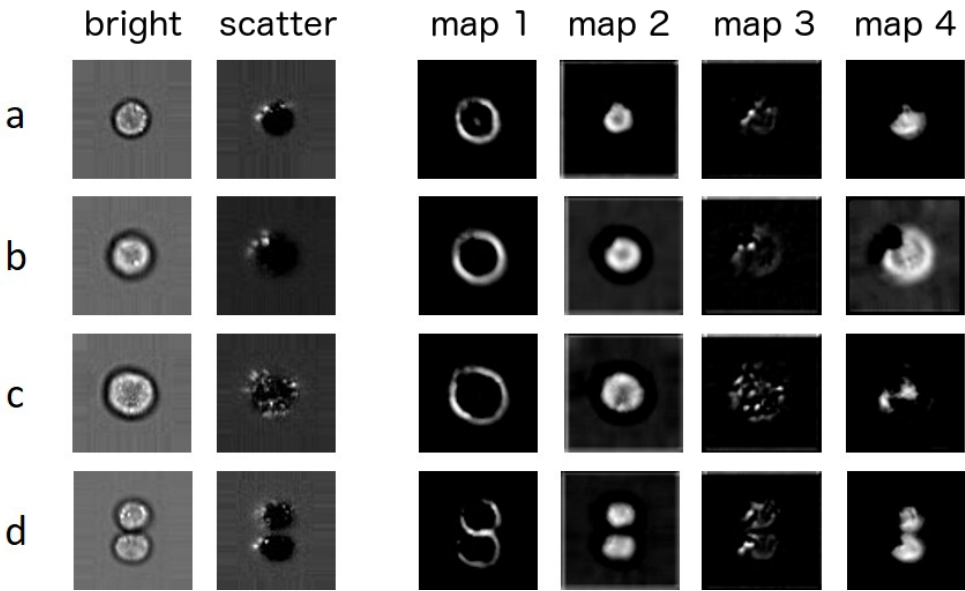


Fig 4. Exemplary activation patterns of intermediate layers. Plotted are activations after the second convolutional module for examples of single cells from four different phases: **a**, G1 **b**, G2 **c**, Anaphase and **d**, Telophase. The response maps mark regions of high activation. Map 1 responds to the cell boundaries. Map 2 responds to the internal area of the cells. Map 3 extracts the localized scatter intensities. Map 4 constitutes a cross-channel feature, which correlates with the difference of map 2 and 3.

DeepFlow detects abnormal cells. 150

Both tSNE visualizations (Fig. 3a,b) produce a small, separate cluster, highlighted with an arrow in Fig. 3b. This cluster is learned in an unsupervised way as cell cycle phase labels provide no information about it: it contains cells from all three interphase classes. While cells in the bulk have high circularity and well defined borders (Fig. 3c), cells in the small cluster are characterized by morphological abnormalities such as broken cell walls and outgrowths, signifying dead cells (Fig. 3d). 151
152
153
154
155
156

Comparison with previous approaches. 157

For comparison, we show the tSNE visualization of cells from the interphase classes in a space of image-analysis based features (Fig. 3e), used in Ref. [5]. The data is neither organized in a continuous way that reflects cell cycle progression, nor can one detect a cluster of abnormal cells. 158
159
160
161

Analysis of intermediate-layer activation patterns. 162

We interpret the data representation encoded in one of the trained intermediate layers of the neural network by inspecting its activation patterns using exemplary input data from several classes (Fig. 4). These activation patterns are the essential information transmitted through the network. They show the response of various kernels on their input. By inspecting the activation patterns, we obtain an insight into what the network is “focusing on” in order to organize data. We observe a strong response to features that arise from the cell border thickness (Fig. 6, map 1), to area-based features 163
164
165
166
167
168
169

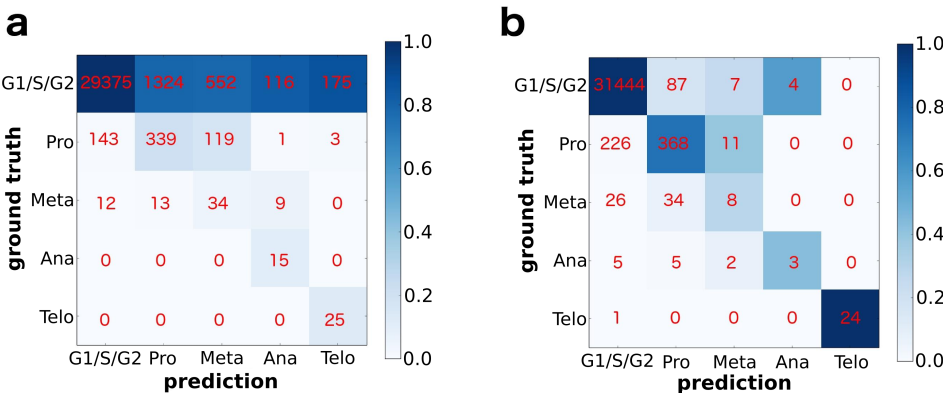


Fig 5. Confusion matrices for boosting and DeepFlow for classification of five classes. To compare with previous work [5], the three interphase phases (G1, S, G2) are treated as a single class. Red numbers denote absolute numbers of cells in each entry of the confusion matrix, that is, diagonal elements correspond to precision. Coloring of the matrix is obtained by normalizing absolute numbers to column sums. **a**, Boosting [5], which leads to 92.35% accuracy. **b**, DeepFlow, which leads to 98.73% \pm 0.16% accuracy.

(Fig. 6, map 2), as well as cross-channel features. For example, map 4 in Fig. 6 shows high response to the difference of information from the brightfield channel, as seen in map 2, and scatter intensities, as seen in map 3. A strong response of the neural network to area-based features as in map 2 could indicate that the network learned to perform a segmentation task.

DeepFlow outperforms boosting for cell cycle classification.

We study the classification performance of DeepFlow on the validation data set shown in Fig. 3. We first focus on the case in which G1, S and G2 phases are considered as a single class. Using five-fold cross-validation on the 32,266 cells, we obtain an accuracy of 98.73% \pm 0.16%. This means a 6-fold improvement in error rate over the 92.35% accuracy for the same task on the same data in prior work using boosting on features extracted via image analysis [5]. The confusion matrix obtained using boosting show high true positive rates for the mitotic phases (Fig. 5a). For example, no cells in Anaphase and Telophase are wrongly classified, as indicated by the zeros in the off-diagonal entries of the two lower rows of the matrix (Fig. 5a). This means high *sensitivity*, most cells from mitotic phases are correctly classified as such. Still this comes at the price of low *precision*: many cells from the interphase class are classified as mitotic phases, as indicated by the high numbers in the off-diagonal entries of the first row of the matrix (Fig. 5a). DeepFlow, by contrast, achieves high sensitivity and precision, leading to an almost diagonal confusion matrix (Fig. 5b).

DeepFlow enables separation of all seven cell cycle classes.

We also evaluated the full seven-class problem in which the three interphase classes are considered individually. Here, we obtain an accuracy of 79.40% \pm 0.77%. This number serves as an orientation for what deep learning could be able to achieve on this particularly hard classification problem — G1, S and G2 are extremely difficult to distinguish (see Fig. 2), even when using information from the fluorescence channels. The accuracy might therefore be affected by wrong labelling, it might be higher if all

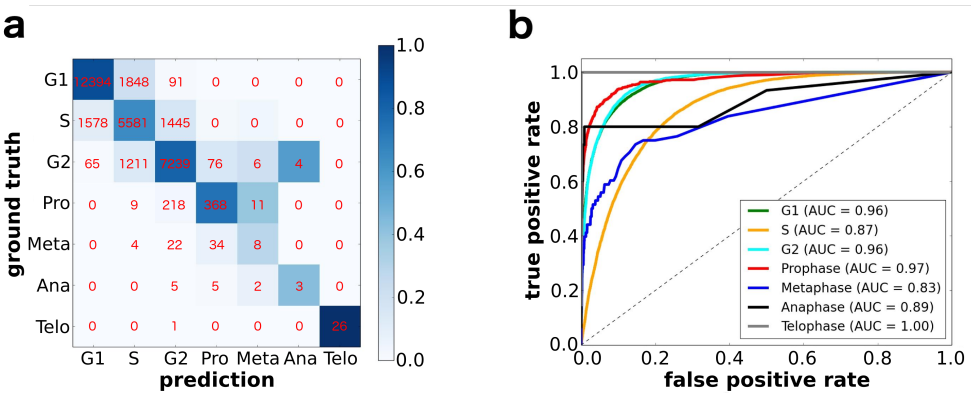


Fig 6. Performance of DeepFlow for classification of seven classes. **a**, Confusion matrix. Red numbers denote absolute numbers of cells in each entry of the confusion matrix. Coloring of the matrix is obtained by normalizing absolute numbers to column sums, that is, diagonal elements correspond to precision. **b**, Class-specific Receiver Operating Characteristics.

fluorescence channels were used as input for the neural network, and it might be slightly lower if “bleed through” enriched brightfield and darkfield images. If high classification accuracy is of importance, and one is not only interested in visualizing and interpreting the data, these questions have to be answered from case to case. Their answer depends in particular on how labels are generated and how many channels of the IFC are used.

Here, we confirm that the considerably lower accuracy as compared to the five-class problem results primarily from cells in the S phase being wrongly classified as either G1 or G2 (Fig. 6a). This is also shown by the Receiver Operating Characteristic, which relates the true positive rate (sensitivity) with the false positive rate (fall-out) as the classification threshold changes (Fig. 6b). Integrating the curve to obtain the standard performance metric “Area under the curve” (AUC). Even though the AUC for the S phase is still high with 0.87, it is the lowest among the majority classes (G1,S,G2), and therefore has a strong effect on the accuracy. Overall we find that all seven classes yield high values, greater than 0.85, and four of the seven classes, yield very high values, greater than 0.95.

Discussion

The visualization of the data as encoded by the last layer of the network using tSNE demonstrates how DeepFlow overcomes a well known issue of traditional machine learning. When trained on a continuous biological process using discrete class labels, conventional machine learning often fail to resolve the continuum [4]. We confirmed this for the present data set of cell-cycling Jurkat cells (Fig. 3e), but note that resolving the continuous cell cycle progression based on features such as those of Ref. [5], has recently been enabled [18] by combining feature extraction with an elaborate trajectory learning algorithm [19]. While this approach still suffers from many other disadvantages of traditional machine learning, as mentioned before, DeepFlow’s approach is conceptually much simpler. The learned features of the neural network — which can also be used for classification — directly generate a feature space, in which data is continuously organized [20]. DeepFlow learns in an unsupervised way that some cells within the G1 phase are at the very beginning of the cell cycle, whereas others in the G1 are already transitioning into the S phase. This is possible as adjacent classes are morphologically

more similar to each other than classes that are temporally further separated. Of course, if this assumption of continuity fails, then DeepFlow will not reconstruct the continuous progression, a limitation in common with the other mentioned algorithmic approaches [18]. Also, note that DeepFlow's simple reconstruction of a continuum is quite exceptional compared to other fields of single-cell biology. For example, in the analysis of single-cell transcriptomic and proteomic data, much research effort has been applied to solve precisely this task [19, 21, 22].

The unsupervised detection of a discrete cluster of abnormal cells indicates that the network learns the cluster of abnormal cells independently of the cell-cycle-label based training. The model is therefore not only capable of resolving the biological process of the cell cycle, but generates features that are general enough to separate even incorrectly labeled cells, which do not belong to this process. This shows the ability of DeepFlow to find completely unknown phenotypes and processes without knowledge about features or even labels in cell populations from IFC data. There is also a high practical use of the detection of damaged cells. The data set used in this paper has been preprocessed using the IDEAS® (Merck Millipore Inc.) analysis software to remove images of abnormal cells. In particular, we removed out of focus cells by gating for images with gradient RMS and debris by gating for circular objects with a large area. The discovery of a cluster of abnormal cells shows the limitations of this approach and provides a solution to it.

An advantage of using a neural network for cell classification in IFC is its speed. Traditional techniques rely on image segmentation and measurement, time-consuming processes limited to roughly 10 cells per second. Neural network predictions, by contrast, are extremely fast, as the main computation consists in parallelizable matrix multiplications ("forward propagations"), which can be performed using optimized numeric libraries. This yields a roughly 100-fold improvement in speed to about 1000 cells per second with a single GPU. Aside from much faster analysis of large cell populations, this opens the door to "sorting on the fly": imaging flow cytometers currently do not allow physically sorting individual cells into separate receptacles based on measured parameters, due to these speed limitations.

Conclusion

Given the compelling performance on reconstructing the cell cycle, we expect DeepFlow to be helpful for a wide variety of biological processes involving continuous morphology changes. Examples include developmental stages of organisms and the progression of healthy states to disease states, situations that have often been non-ideally reduced to binary classification problems. Ignoring intrinsic heterogeneity has likely hindered a deeper insight into the mechanisms at work. In an example where we studied the progression from healthy to diseased states, preliminary results indicate that DeepFlow resolves and visualizes this process well when using brightfield, darkfield and fluorescence channels as input for the network. Analysis as demonstrated here could reveal morphological signatures in optical and fluorescence channels at much earlier stages than previously recognized.

We also expect DeepFlow to be helpful for a wide variety of image data, including images from high-throughput microscopy. Although generally lower-throughput in terms of the number of cell processed, conventional microscopy is nevertheless still high-throughput and can usually provide higher resolution images than IFC, providing advantages for some biological processes. Furthermore, given that multi-spectral methods are advancing rapidly, imaging mass spectrometry is allowing dozens of labeled channels to be acquired [23, 24]. Due to its basic structure and high flexibility, DeepFlow can accommodate a large increase in the number of available channels.

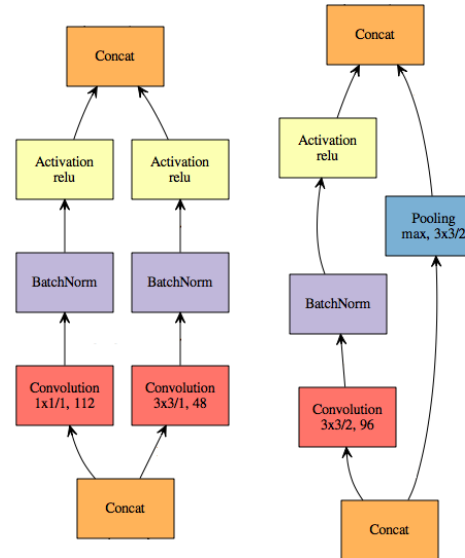


Fig 7. Dual-path modules. **a**, Normal dual-path Module. **b**, Reduction dual-path Module. The numbers beneath the convolution operations indicate the kernel sizes, stride and the number of filters.

Although the current version of DeepFlow is oriented towards those with computational expertise, a biologist-oriented version could be created to make the general approach more tractable to that audience. The packages used for this paper are listed in the supplemental notes.

Acknowledgments

F.A.W. acknowledges support by the “Helmholtz Postdoc Programme”, Initiative and Networking Fund of the Helmholtz Association. P.R. and A.E.C. acknowledge the support of the Biotechnology and Biological Sciences Research Council/ National Science Foundation under grant BB/N005163/1 and NSF DBI 1458626.

Supplemental Notes

Preprocessing.

Our algorithmic workflow of cell cycle analysis with Deep Neural Networks begins with brightfield and darkfield images from the cells. In order to allow uniform training of our network on the whole dataset, we resize the images to 66×66 pixels by stretching the border pixels. We choose this method over individual image rescaling to avoid the destruction of possibly important size relation information between cells.

The data set used in this paper has been preprocessed using the IDEAS® software (Merck Millipore Inc.) to remove images of abnormal cells. In particular, we removed out of focus cells by gating for images with gradient RMS and removed debris by gating for circular cells with a large area.

Network architecture.

Figure 7 shows normal and reduction dual-path modules, the basic elements of the network architecture of DeepFlow discussed in the main text. Kernel sizes, stride and number of filters are indicated in the figure.

The DeepFlow network architecture consists of 42 layers, which results in a total number of parameters of about 2 mio. It is build up starting with 3 dual-path reduction modules, followed by 10 normal dual-path modules, one pooling layer, one fully connected layer and the softmax layer. Each dual-path module consists in 3 layers: a convolution layer, a batch normalization layer and an activation layer. Although there is no “big” fundamental difference between dualpath and standard convolution modules, dual-path based networks tend to converge a little better in practice, since the gradient flow from pooling and convolution in the reduction module counteracts the vanishing gradient problem: not the entire gradient gets multiplied by approx 10^{-4} convolutional weight, pooling just lets it through.

In the first (input) layer, all IFC channels are combined in a linear operation by feeding them in the channel — which equals the color — dimension of the convolution input. This means the convolution uses kernels which convolve over all channels simultaneously. The number of 3×3 kernel weights then is nine times the number of channels. Increasing the number of channels simply increases the “kernel depth” in the color dimension, and hence, is trivial.

Training details.

The network was trained for 100 epochs using stochastic gradient descent with standard parameters: 0.9 momentum, a fixed learning rate of 0.01 up to epoch 85 and of 0.001 afterwards as well as a slightly regularizing weight decay of 0.0005. Training took around 7 h and was stopped manually by inspecting convergence cross-entropy.

Implementation.

For the results presented in this paper, we implemented DeepFlow using the MxNet framework [25] on a NVIDIA Titan X GPU. MxNet is lightweight, fast and memory efficient and available from <https://github.com/dmlc/mxnet>. Due to the fast progress in the development of deep learning software packages, in the meanwhile, we have also implemented and successfully tested our architecture using TensorFlow, which is available from <https://github.com/tensorflow/tensorflow>. The user might choose the software package according to personal preferences.

Nonlinear dimension reduction.

We use the tSNE implementation of Ref. [17] available from <https://lvdmaaten.github.io/tsne>.

Bleed through.

The data acquired using the ImageStream was fully compensated using typical control images (see Ref. [26]) so the image tiffs would have minimal bleed through between channels. We could not detect even a slight indication of bleed through in the Jurkat cell data, neither upon inspection by eye, nor upon correlating the integrated intensity of each fluorescence channel with the integrated intensity of bright and darkfield channels, respectively. We then checked the existence of bleed through in the Cytometer used for data generation by switching off the light source of the brightfield channel, while keeping the fluorescence excitation on. We would then expect zero intensity in the

brightfield images, but instead measured a slight intensity stemming from the fluorescence channels. This common technical aspect of IFC measurements merits an own investigation and will appear elsewhere. Here, our aim is to compare methodologies rather than to claim absolute levels of accuracy.

References

1. Pepperkok R, Ellenberg J. High-throughput fluorescence microscopy for systems biology. *Nature Reviews Molecular Cell Biology*. 2006;7(9):690–696.
doi:10.1038/nrm1979. 342
2. Basiji DA, Ortyn WE, Liang L, Venkatachalam V, Morrissey P. Cellular image analysis and imaging by flow cytometry. *Clinics in Laboratory Medicine*. 2007;27(3):653–670. 343
3. Brown M, Wittwer C. Flow cytometry: principles and clinical applications in hematology. *Clinical chemistry*. 2000;46(8):1221–1229. 344
4. Eliceiri KW, Berthold MR, Goldberg IG, Ibanez L, Manjunath BS, Martone ME, et al. Biological imaging software tools. *Nature Methods*. 2012;9(7):697–710.
doi:10.1038/nmeth.2084. 345
5. Blasi T, Hennig H, Summers HD, Theis FJ, Cerveira J, Patterson JO, et al. Label-free cell cycle analysis for high-throughput imaging flow cytometry. *Nature Communications*. 2016;7:10256. doi:10.1038/ncomms10256. 353
6. Jones TR, Carpenter AE, Lamprecht MR, Moffat J, Silver SJ, Grenier JK, et al. Scoring diverse cellular morphologies in image-based screens with iterative feedback and machine learning. *PNAS*. 2009;106(6):1826–1831.
doi:10.1073/pnas.0808843106. 355
7. Dao D, Fraser AN, Hung J, Ljosa V, Singh S, Carpenter AE. CellProfiler Analyst: interactive data exploration, analysis, and classification of large biological image sets. *Bioinformatics*. 2016;32(20):3210–3212. doi:10.1093/bioinformatics/btw390. 362
8. Chen CL, Mahjoubfar A, Tai LC, Blaby IK, Huang A, Niazi KR, et al. Deep Learning in Label-free Cell Classification. *Scientific Reports*. 2016;6:21471.
doi:10.1038/srep21471. 368
9. Kraus OZ, Ba LJ, Frey B. Classifying and Segmenting Microscopy Images Using Convolutional Multiple Instance Learning. *Bioinformatics*. 2016;32(12):i52–i59.
doi:10.1093/bioinformatics/btw252. 371
10. Pärnamaa T, Parts L. Accurate classification of protein subcellular localization from high throughput microscopy images using deep learning. *bioRxiv*. 2016;doi:10.1101/050757. 374
11. Hennig H, Rees P, Blasi T, Kamentsky L, Hung J, Dao D, et al. An open-source solution for advanced imaging flow cytometry data analysis using machine learning. *Methods*. 2016;doi:10.1016/j.ymeth.2016.08.018. 377
12. Krizhevsky A, Sutskever I, Hinton GE. ImageNet Classification with Deep Convolutional Neural Networks. In: Pereira F, Burges CJC, Bottou L, Weinberger KQ, editors. *Advances in Neural Information Processing Systems 25*. Curran Associates, Inc.; 2012. p. 1097–1105. 380

13. Vincent P, Larochelle H, Lajoie I, Bengio Y, Manzagol PA. Stacked denoising autoencoders: Learning useful representations in a deep network with a local denoising criterion. *Journal of Machine Learning Research*. 2010;11(Dec):3371–3408. 384
385
386
387
14. Szegedy C, Liu W, Jia Y, Sermanet P, Reed S, Anguelov D, et al. Going deeper with convolutions. In: *Proceedings of the IEEE Conference on Computer Vision and Pattern Recognition*; 2015. p. 1–9. 388
389
390
15. LeCun Y, Bengio Y, Hinton G. Deep learning. *Nature*. 2015;521(7553):436–444. 391
doi:10.1038/nature14539. 392
16. Donahue J, Jia Y, Vinyals O, Hoffman J, Zhang N, Tzeng E, et al. DeCAF: A Deep Convolutional Activation Feature for Generic Visual Recognition. *arXiv*. 2013; p. 1310.1531. 393
394
395
17. van der Maaten L, Hinton G. Visualizing Data using t-SNE. *Journal of Machine Learning Research*. 2008;9(Nov):2579–2605. 396
397
18. Gut G, Tadmor MD, Pe'er D, Pelkmans L, Liberali P. Trajectories of cell-cycle progression from fixed cell populations. *Nature Methods*. 2015;12(10):951–954. 398
doi:10.1038/nmeth.3545. 399
400
19. Bendall SC, Davis KL, Amir EaD, Tadmor MD, Simonds EF, Chen TJ, et al. Single-Cell Trajectory Detection Uncovers Progression and Regulatory Coordination in Human B Cell Development. *Cell*. 2014;157(3):714–725. 401
doi:10.1016/j.cell.2014.04.005. 402
403
404
20. Schroff F, Kalenichenko D, Philbin J. FaceNet: A Unified Embedding for Face Recognition and Clustering. *arXiv*. 2015; p. 1503.03832. 405
406
21. Trapnell C, Cacchiarelli D, Grimsby J, Pokharel P, Li S, Morse M, et al. The dynamics and regulators of cell fate decisions are revealed by pseudotemporal ordering of single cells. *Nature Biotechnology*. 2014;32(4):381–386. 407
doi:10.1038/nbt.2859. 408
409
410
22. Haghverdi L, Büttner M, Wolf FA, Buettner F, Theis FJ. Diffusion pseudotime robustly reconstructs branching cellular lineages. *Nature Methods*. 2016;13:845–848. doi:10.1038/nmeth.3971. 411
412
413
23. Bodenmiller B, Zunder ER, Finck R, Chen TJ, Savig ES, Bruggner RV, et al. Multiplexed mass cytometry profiling of cellular states perturbed by small-molecule regulators. *Nature Biotechnology*. 2012;30(9):858–867. 414
doi:10.1038/nbt.2317. 415
416
417
24. Angelo M, Bendall SC, Finck R, Hale MB, Hitzman C, Borowsky AD, et al. Multiplexed ion beam imaging of human breast tumors. *Nature Medicine*. 2014;20(4):436–442. doi:10.1038/nm.3488. 418
419
420
25. Chen T, Li M, Li Y, Lin M, Wang N, Wang M, et al. MXNet: A Flexible and Efficient Machine Learning Library for Heterogeneous Distributed Systems. *arXiv*. 2016; p. 1512.01274. 421
422
423
26. Filby A, Perucha E, Summers H, Rees P, Chana P, Heck S, et al. An imaging flow cytometric method for measuring cell division history and molecular symmetry during mitosis. *Cytometry Part A*. 2011;79A(7):496–506. 424
doi:10.1002/cyto.a.21091. 425
426
427